The transformation of ethanol over $AlPO_4$ and SAPO molecular sieves with AEL and AFI topology. Kinetic and thermodynamic approach

Daniel Arias, Alicia Colmenares, María L. Cubeiro, José Goldwasser, Carmen M. López *, Francisco J. Machado* and Virginia Sazo

Centro de Catálisis, Petróleo y Petroquímica, Facultad de Ciencias, UCV, Apdo. 47102, Caracas 1020-A, Venezuela
E-mail: {fmachado, cmlopez}@strix.ciens.ucv.ve

M.M. Ramírez de Agudelo

INTEVEP, S.A.

Received 13 December 1996; accepted 4 March 1997

The transformation of ethanol into ether and ethylene was studied over a series of aluminophosphates and silicoaluminophosphates with AFI and AEL topology, at 593 K. It was found that the data followed a simple parallel kinetic scheme. The formation of ether, the less demanding reaction, can be strongly limited by thermodynamics. Based on both the kinetic model and the equilibrium curve for the system considered, a series of parameters were defined in order to determine the relative strength and concentration of the active centres participating in both reactions. Differences in the average specific-activity for the ethanol transformation into ethylene (turnover-like number) were rationalised in terms of differences in the average hydrogen-atoms partial-charge. Structural influence on product distribution due to the shape-selective phenomenon was not observed under the reaction conditions employed.

Keywords: ethanol transformation, $AlPO_4$-molecular sieves, thermodynamics, kinetics, acidity

1. Introduction

The transformation of ethanol over acid solids has been widely studied [1–4]. There seems to be a general agreement on the fact that both ethyl ether and ethylene are primary products. Ethylene formation appears to be the more demanding reaction requiring, as a result, stronger acid sites [5–7]. Ethylene can also be obtained as a secondary product from the consecutive transformation of the ethyl ether first formed [2,8]. Further transformation of the ethylene formed into hydrocarbons of higher molecular weight is likely to occur over solids, such as ZSM-5, containing very strong acid sites [3,4].

Previous thermodynamic calculations have shown that the formation of ether as a final product is strongly unfavoured, over a whole range of temperatures studied, with respect to the olefin production [9]. Therefore, care must be taken when interpreting the variation of product distribution in terms of catalyst selectivity alone, without considering the role the thermodynamic equilibrium might be playing on such product distribution.

By assuming a second-order reaction for the formation of ether and first-order reaction for the formation of ethylene in a parallel kinetic scheme, a linear correlation between the ratio ether/ethylene (E/O) and the unconverted fraction of ethanol $(1 - X)$ should be expected, as shown by the following equation:

$$\mathrm{E/O} = (k_e/k_o)P_{ao}(1 - X)\,, \qquad (1)$$

where k_e and k_o represent the rate constants for the transformation of ethanol into ether and ethylene, respectively. X represents the total fractional conversion of ethanol and P_{ao}, the ethanol pressure in the feed stream. Therefore, by representing the observed E/O ratio as a function of $(1 - X)$ straight lines of intercepts at zero should be obtained under a kinetic regime for a given initial partial pressure of ethanol. On the other hand, by allowing different degrees of extension for the reaction leading to olefin from a given initial ethanol partial pressure, the resulting equilibrium yield to ether can readily be determined from a typical thermodynamic treatment. Under these circumstances, a clear picture of the reaction regime can be obtained at each conversion level as a function of the space velocity. In this way the interpretation of product distribution can be done with a higher degree of confidence.

The main purpose of this paper is to evaluate the potential application of the ethanol transformation as a test to characterise the surface acidity and the selectivity behaviour of aluminophosphate-based molecular sieves. In order to do so, the influence of thermody-

* To whom correspondence should be addressed.

namics and kinetics on the product distribution will be examined.

2. Experimental

2.1. Sample preparation and characterisation

A detailed synthesis procedure for the preparation of $AlPO_4$-11 and SAPO-11 was given in a previous paper [10]. For the structure AFI the synthesis procedure was analogous to the previous one with the exception of the organic template that, in this case, was triethylamine. Typical synthesis conditions of the solids studied are given in table 1.

Al and P contents of the solids were determined with the aid of an atomic emission spectrometer, having an inductively coupled plasma source. Si content was analysed by atomic emission spectrometry. The percentage of crystallinity was determined from the X-ray diffractograms recorded, after calcination overnight at 773 K of the synthetic solids, with a Philips diffractometer PW 1730 using Co-Kα radiation ($\lambda = 1.790255$ Å) operated at 30 kV, 20 mA and scanning speed of 2° 2θ/min. Diffraction lines between 8 and 25° 2θ were taken as reference for this calculation. N_2-specific surface areas (SSA) were obtained with a Micromeritics 2200 sorptometer at liquid nitrogen temperature, after pre-treating the samples in situ at 623 K under vacuum for 3 h.

2.2. Acidity measurement

Surface acidity was determined using pyridine as the probe base. Pyridine temperature-programmed desorption (TPD) experiments were carried out with the aid of a Micromeritics equipment model 2900. First, the solid sample was pre-treated at 788 K for 30 min under a dry He stream. Then, the sample was cooled down and saturated with pulses of pyridine at 443 K. Finally, the desorption of the pyridine chemisorbed was done from 443 to 788 K at a heating rate of 10 K per min under a He-flow of 30 $cm^3\ min^{-1}$.

FTIR of the pyridine/catalyst interaction was also done. Self-supporting wafers of 7 mg/cm^2 were placed in an IR-cell specially designed for gas and thermal in situ treatments and activated under vacuum (10^{-5} Torr) at 723 K overnight. Afterwards, the temperature was dropped to 363 K and pyridine was admitted to the cell (5 Torr). Then, the excess pyridine was evacuated. All the spectra in the pyridine region were recorded after outgassing at 443 K. The intensity of the bands (band area/wafer optic density) at 1550 (I_B) and 1450 cm^{-1} (I_L), measured after reaching the outgassing temperature, were taken as to be proportional to the concentration of Brønsted and Lewis acid sites, respectively. In order to quantify the fraction of Brønsted sites the integrated molar extinction coefficients (IMEC) obtained by Emeis [11] were used to correct the band-intensities as follows:

$$\mathrm{B}/(\mathrm{B}+\mathrm{L}) = I_B/[(I_B/1.67) + (I_L/2.22)] = 1/[1 + 0.752(I_L/I_B)]\,, \qquad (2)$$

where 2.22 and 1.67 (cm/μmol) are the IMEC for the Lewis and Brønsted bands respectively. By combining both techniques, the number of each kind of acid sites per unit cell could be readily obtained. For the purpose of this work the total acidity in terms of the acid strength was arbitrarily defined as those sites retaining pyridine at 443 K. Acid sites of higher strength, associated with those sites desorbing pyridine above 623 K, have been taken from pyridine-TPD thermograms.

Table 1
Synthesis conditions and nomenclature of the solids studied as used in this work [a]

Solid	Gel molar composition	T_c (K)	t_c (h)
SAPO-11	Al_2O_3:P_2O_5:0.3SiO_2:DPA:50H_2O	473	24
$AlPO_4$-11	Al_2O_3:P_2O_5:DPA:50H_2O	473	24
SAPO-5	Al_2O_3:P_2O_5:0.4SiO_2:Et_3N:50H_2O	473	24
$AlPO_4$-5	Al_2O_3:P_2O_5:Et_3N:50H_2O	473	24

[a] T_c, and t_c: temperature and time of crystallisation, respectively. DPA: di-*n*-propylamine, Et_3N: triethylamine.

2.3. Catalytic test

The chemical transformation of ethanol was carried out at 593 K in a continuous flow glass reactor under atmospheric pressure. Nitrogen was used as a carrier gas at a molar ratio N_2/ethanol of 11.5 and ethanol partial pressure of 0.08 atm. A typical space velocity (WHSV) of 3.3 h^{-1} (grams of ethanol per hour per gram of catalyst) was calculated at 298 K and 1 atm. In order to check for the kinetics scheme proposed the space velocity was varied between 1.6 and 32 h^{-1} by changing the carrier-gas flow rate over the same catalyst sample. At least two analyses were taken for each WHSV over a period not exceeding 10 min-on-stream. In all cases, the weight of catalyst employed was about 0.1 g. Before the reaction, the samples were activated at 693 K for 3 h under dry-N_2 stream. Products were analysed in line by FID-GC using a Porapak T packed-column of 3 m length and 1/8 inch diameter.

2.4. Kinetic and thermodynamic calculations

The following parameters were calculated assuming the stoichiometry of the kinetic parallel scheme proposed:

(a) Total ethanol conversion (X):

$$X = (X_o + 2X_e)/(X_o + 2X_e + X_a)\,, \qquad (3)$$

where X_o, X_e and X_a represent the molar fraction of olefin (ethylene), ether and alcohol (ethanol) in the product stream.

Table 2
Some characteristics of the solids studied

Sample	SSA (m^2/g)	V_p [a] (cm^3/g)	%Cryst.	Molar composition formula TO_2
SAPO-11	124	0.044	70	$(Al_{0.47}P_{0.47}Si_{0.06})O_2$
$AlPO_4$-11	116	0.041	100	$(Al_{0.5}P_{0.5})O_2$
SAPO-5	323	0.115	100	$(Al_{0.49}P_{0.43}Si_{0.08})O_2$
$AlPO_4$-5	351	0.125	90	$(Al_{0.51}P_{0.49})O_2$

[a] $V_p\,(cm^3/g) = 3.55 \times 10^{-4}\,SSA\,(m^2/g)$.

(b) Yield to olefin (Y_o) and ether (Y_e):

$$Y_o = X_o/(X_o + 2X_e + X_a)\,, \quad (4)$$

$$Y_e = X_e/(X_o + 2X_e + X_a)\,. \quad (5)$$

The ether to olefin ratio (E/O) was evaluated from the previous values.

(c) Equilibrium curve: The equilibrium curves were calculated from the values of the equilibrium constants for both the formation of ether ($K_e = 3$) and the formation of olefin ($K_o = 512$). These equilibrium constants were determined from the corresponding Gibbs expressions, using the values of ΔG^0 at 600 K for each reaction (-1.31 and -7.41 kcal mol^{-1} for ether and ethylene formation respectively) which were, in turn, calculated from the values of ΔG_f^0 at 600 K for each compound as reported by Stull [12].

3. Results and discussion

3.1. Characterisation

Some characteristics of the solid studied are given in table 2. The molar composition, expressed in terms of formula TO_2, was obtained by taking the average of three different chemical analyses. The result for $AlPO_4$-5 suggests a small excess of Al, probably as extra-framework alumina. The N_2-sorption capacities of all the samples, as inferred from the SSA values and pore volumes, are within the range (0.02–0.05 cm^3/g for AEL and 0.09–0.13 cm^3/g for AFI) previously reported for these structures [13,14]. However, higher adsorption capacities, close to 200 $m^2\ g^{-1}$ (0.07 cm^3/g) have also been reported for AEL-like molecular sieves [15]. Moreover, different preparations of $AlPO_4$-11 in our own laboratory have showed SSA values as high as 167 m^2/g, corresponding to a pore volume of 0.06 cm^3/g (see table 2 of ref. [10]). These differences in sorption capacity are not apparently associated to crystallinity loss. Instead, the presence of some residual extra-framework material from the synthesis, causing a partial blockage of the pores, might be occurring. This extraneous material should be in a small proportion since they were undetected by XRD. In fact, as illustrated in figure 1, neither extra-lines corresponding to different crystalline cophases nor significant background suggesting the coexis-

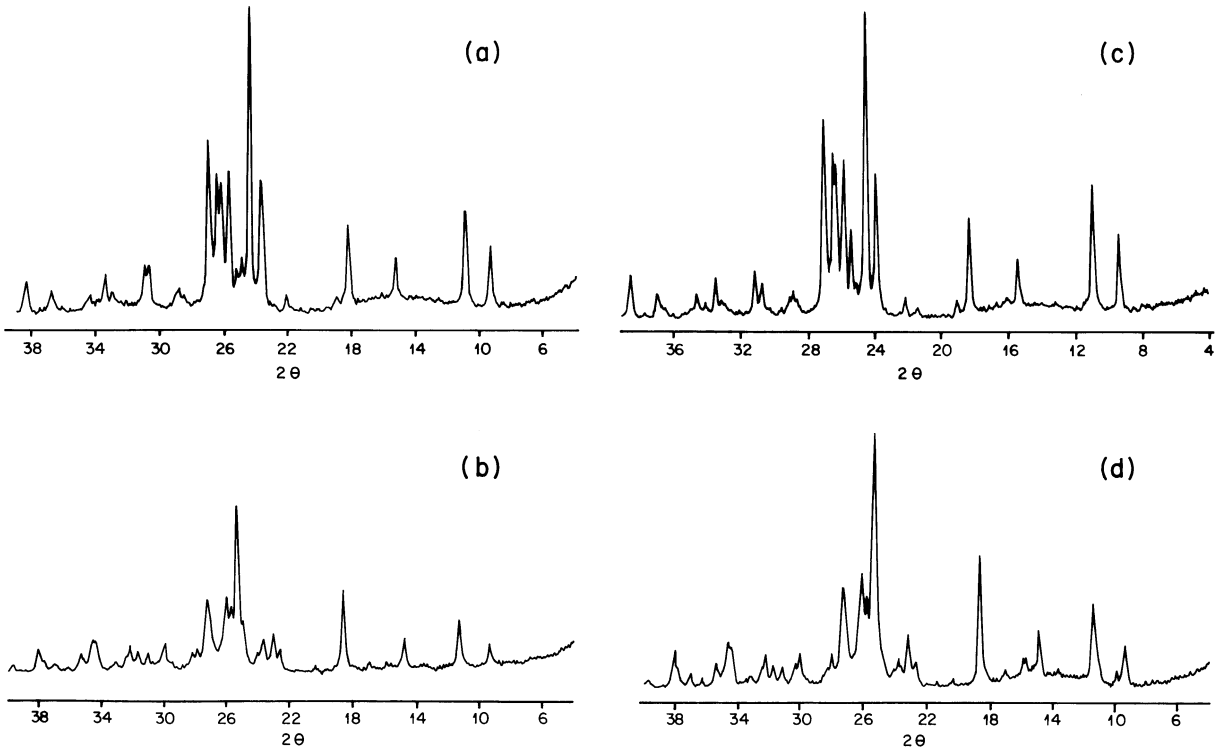

Figure 1. X-ray diffractograms of the AEL-like materials. (a) SAPO-11 as-prepared; (b) SAPO-11 calcined; (c) $AlPO_4$-11 as-prepared; (d) $AlPO_4$-11 calcined.

Table 3
Acidity measurements from pyridine-TPD and pyridine-IR techniques

Catalyst	Pyridine-TPD (mmol/g)			Pyridine-IR (AU)		
	443–623 K	623–786 K	total	I_B	I_L	B/(B + L) [a]
$AlPO_4$-5	0.175	0.089	0.264	2.47	4.10	0.44
$AlPO_4$-11	0.149	0.040	0.189	3.40	4.59	0.50
SAPO-5	0.252	0.324	0.576	9.02	4.41	0.73
SAPO-11	0.132	0.186	0.318	3.32	3.83	0.54

[a] Calculated from eq. (2).

tence of an amorphous phase, could be appreciated from the X-ray diffractograms of the AEL samples, recorded before and after calcination. Differences in the XRD patterns of the calcined samples, associated with changes in the crystal symmetry from a body-centred to a primitive unit cell, have already been reported and discussed previously [10,16].

^{29}Si MAS NMR technique has previously been used to verify the incorporation of Si in the framework [10,17]. For SAPO-5 (AFI topology) a main signal was observed at about −90 ppm, typical of Si(4Al) entities. By contrast, a main band at −112 ppm, related to "silicon islands", was found for SAPO-11 (AEL topology). The previous result indicates that different mechanisms of Si incorporation in the framework are occurring. The fact that the Si atomic fraction is very similar for both structures (see table 2) suggests that the mechanism of Si incorporation depends on the crystal topology. Thus, whereas in the AFI structure the prevailing mechanism of substitution appears to be SM2, for AEL it seems to be SM2 + SM3. The implication of the type of Si incorporation on the acidity of the resulting SAPO was already discussed [10]. For an equal Si loading, substitution via SM2 + SM3 leads to a smaller number of acid sites per Si atom incorporated but of higher strength as compared with the SM2 mechanism. The higher the Si content the greater the difference in acidity resulting from these two types of substitution.

3.2. Acidity

Results of the acidity measurements are given in table 3. Both pyridine-TPD and pyridine-IR data are reported. As seen from TPD, the total amount of pyridine desorbed between 443 and 786 K was about twice as much for SAPO's as compared with their corresponding AlPO's. For the former the fraction of sites desorbing pyridine above 623 K represents about 60% whereas for the latter it ranges from 20 to 35%. SAPO-5 showed about 80% higher total pyridine chemisorption than SAPO-11, which is in agreement with the value calculated from the summation of the corrected IR-bands at 443 K $[(I_B/1.67) + (I_L/2.22)]$. At this temperature the amount of Brønsted sites in SAPO-5 calculated from IR is as much as 2.7 times higher than the one in SAPO-11. This ratio can be compared with the one obtained by combining TPD and IR data which is 2.5. By combining the pyridine-TPD and pyridine-IR data of table 3 the following series in terms of the total Brønsted acidity (mmol pyridine/g catalyst) was observed:

$$\text{SAPO-5 (0.42)} > \text{SAPO-11 (0.17)} > \text{AlPO}_4\text{-5 (0.11)} \approx \text{AlPO}_4\text{-11 (0.10)}.$$

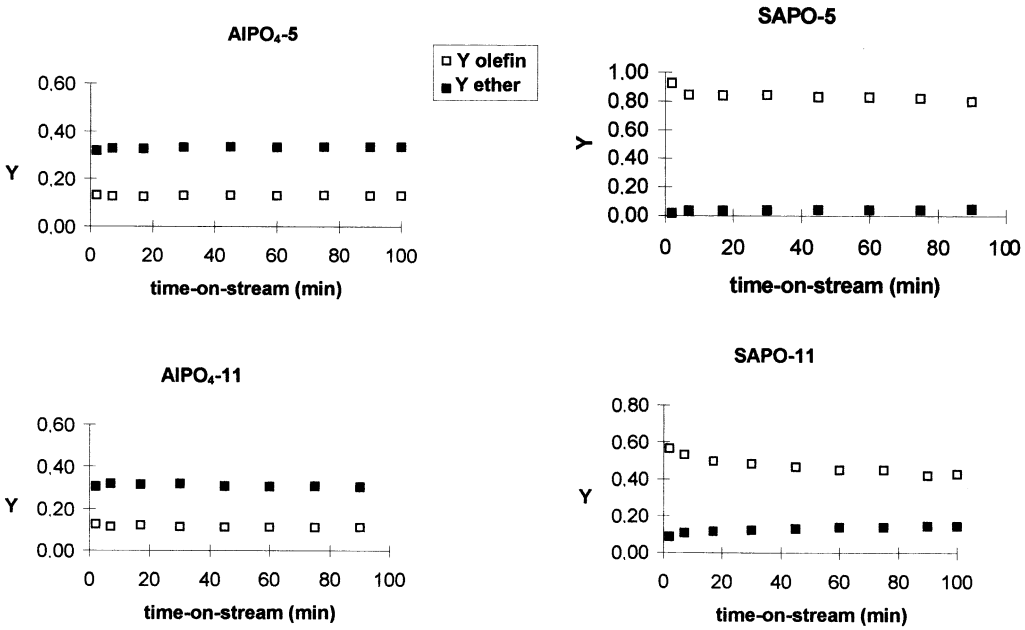

Figure 2. Selectivity and deactivation curves during the first 100 min-on-stream for the transformation of ethanol over SAPO's and AlPO's with the AEL and AFI structure, measured at 593 K and WHSV of 3.3 h^{-1}.

Table 4
Average product distribution measured at different WHSV over a period of 10 min-on-stream. See experimental section for additional details

WHSV (h^{-1})	$AlPO_4$-5			$AlPO_4$-11			SAPO-5			SAPO-11		
	X_a	X_e	X_o	X_a	X_e	X_o	X_a	X_e	X_o	X_a	X_e	X_o
1.6	0.26	0.43	0.31	0.30	0.42	0.28	–	–	–	0.06	0.03	0.91
3.3	0.34	0.47	0.19	0.38	0.44	0.18	0.06	0.01	0.93	0.19	0.13	0.67
4.0	0.37	0.46	0.16	0.42	0.43	0.15	–	–	–	–	–	–
8.1	0.52	0.39	0.09	0.57	0.35	0.08	0.16	0.03	0.81	0.45	0.21	0.34
16.2	0.66	0.29	0.05	0.71	0.25	0.04	0.41	0.06	0.53	0.61	0.19	0.20
32.0	–	–	–	–	–	–	0.55	0.06	0.39	–	–	–

Surface acidity in $AlPO_4$ structures, supposed to be neutral, has largely been observed even in highly pure and crystalline materials [18–20]. This extraneous behaviour has been associated to structural defects leading to P-OH and Al-OH groups [20,21]. The exact nature of these sites is, however, still unclear.

3.3. Ethanol transformation

Deactivation–selectivity curves for the catalysts studied over a period 100 min-on-stream and at a WHSV of 3.3 h^{-1} , are given in figure 2. From this figure the high stability of both structures towards deactivation, regardless of their acidity level, can be appreciated. This behaviour is a clear indication that consecutive transformations of the primary products to higher hydrocarbons and coke do not play a significant role. Differences in product selectivity are clearly evidenced. The calculated absolute-maximum theoretical-yield for ether at 600 K, corresponding to the equilibrium value when only the transformation to ether occurs (Y_o = zero), is 0.39. For ethylene formation, having an equilibrium constant 171 times higher than the ether one, there is no thermodynamic limitation, under our experimental conditions. An olefin restriction factor (ORF) can, therefore, be defined as the ratio of the actual ether yield (Y_e) to the absolute-maximum theoretical-yield (0.39). This factor will represent an estimation of the catalyst restriction for the ethanol dehydration to ethylene to occur. The higher this factor the higher the catalyst restriction. It is evident from figure 1 that both non-substituted AlPO's showed the highest olefin restriction factor (ORF $\approx$ 0.85). In contrast, the olefin restriction factor for SAPO's was very poor. SAPO-5 showed the lowest (ORF $\leqslant$ 0.13) whereas for SAPO-11 the parameter ORF reached 0.38 as a maximum.

Average molar fractions for alcohol (X_a), ether (X_e), and olefin (X_o) in the product stream, measured at different WHSV over a period of 10 min-on-stream, are presented in table 4. From these data the total conversion (X), the ether and olefin yields (Y_e and Y_o) and the ether to olefin ratio (E/O) can be readily calculated from eqs. (3)–(5). The ether to olefin ratio (E/O) as a function of the ethanol unconverted fraction ($1 - X$) is represented in figure 3. The calculated equilibrium data were also plotted (dashed line). Due to marked differences in the E/O values between AlPO's and SAPO's, separate graphs are shown (please notice the difference in the y-axis scales). As seen from these plots, linear correlations between E/O and ($1 - X$) were obtained, apparently in agreement with eq. (1) derived from the parallel scheme proposed for the ethanol transformation. The corresponding linear least-squares expressions are inserted in the respective graphs of figure 3. SAPO-5, with the highest olefin selectivity (very low E/O ratio), showed the better fit in spite of the fact that, at least, one out of their four data-points is at equilibrium. This observation can be understood by examining the shape of the equilibrium curve. This curve asymptotically approaches zero at

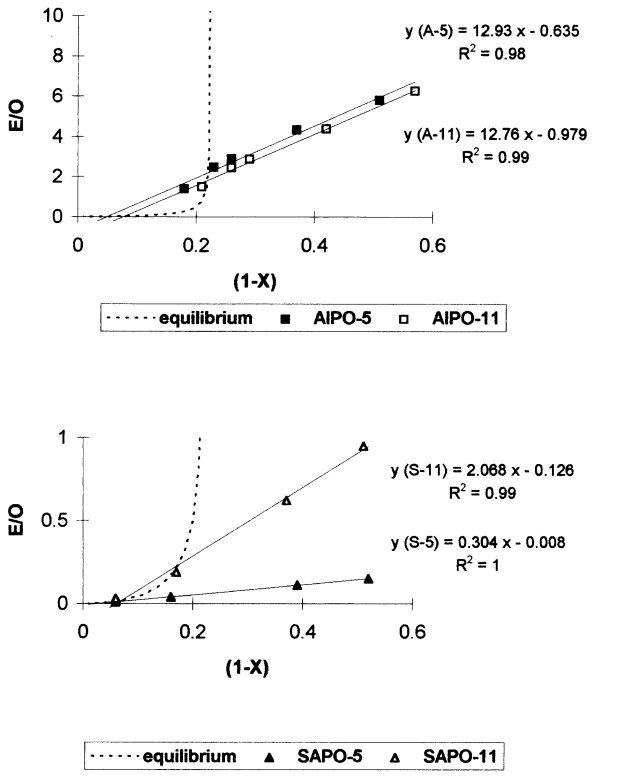

Figure 3. Ether-to-olefin ratio as a function of the ethanol unconverted fraction. Notation A-5, A-11, S-5 and S-11 in the linear least-squares expressions correspond to the catalysts $AlPO_4$-5, $AlPO_4$-11, SAPO-5 and SAPO-11, respectively. Equilibrium curve is represented by the dashed line.

values of $(1 - X) < 0.2$. In this range the equilibrium curve becomes a straight line, coinciding with the one of the least-squares expression derived for SAPO-5. By contrast, at a value of $(1 - X)$ of about 0.22 the equilibrium curve asymptotically goes to ∞. Consequently, for those catalysts more selective to ether (c.a. E/O above 1), the experimental data taken at or near equilibrium conditions are expected to deviate from linearity as they fall in the equilibrium curve (see figure 3). In fact, as seen from the least-squares expression inserted in the graphs of figure 3, the intercepts deviation from zero for the AlPO's correlations (-0.635 and -0.979 for $AlPO_4$-5 and $AlPO_4$-11, respectively) is higher than the one observed for SAPO-5 (-0.008). The situation for SAPO-11 (-0.126) is somewhere in between the two previous cases.

A better picture of the previous behaviour can be obtained from figure 4. In this figure the ether yield, Y_e, has been plotted as a function of the olefin yield, Y_o. The equilibrium values are represented by the dashed line. It is worthy to remind that each experimental point was measured by changing the WHSV, being those data closer to the equilibrium curve the ones obtained at the lower WHSV. It can be observed that the ether yield for the ether selective catalysts (AlPO's) increases more rapidly than the olefin yield until the equilibrium is reached. Then, as expected, it drops to follow the equilibrium curve. The situation is reversed for SAPO's and the rate of olefin production becomes much higher than the rate of ether formation. As in the previous case, the experimental data at the lower WHSV are adjusted to the equilibrium curve. Straight-lines have been arbitrarily traced through the experimental points of SAPO-11 and SAPO-5, located far from the equilibrium, to roughly estimate the cutting point at the equilibrium curve. It can be observed that each catalyst reaches the equilibrium curve at a specific Y_o-value. The higher this value the higher the olefin selectivity. According to this criterion the following olefin selectivity series was obtained:

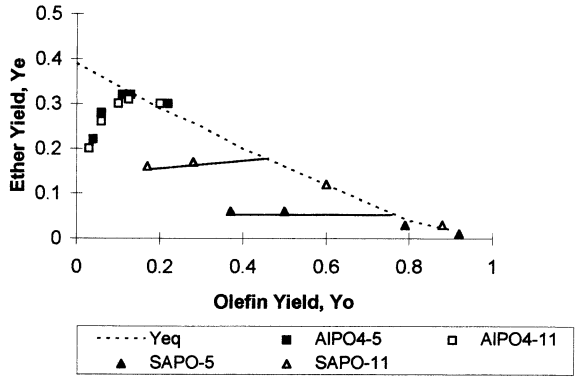

Figure 4. Ether yield as a function of the olefin yield. Equilibrium curve is represented by the dashed line.

$$\text{SAPO-5}\ (Y_o \approx 0.75) > \text{SAPO-11}\ (Y_o \approx 0.45) > \text{AlPO}_4\text{-5} \approx \text{AlPO}_4\text{-11}\ (Y_o \approx 0.15)\,.$$

It seems from the previous discussion that the transformation of ethanol into ethylene occurs over acid sites with higher acid strength than those required for the ether formation.

The reciprocal of the slopes of the straight lines shown in figure 3 can be taken as a measure of the concentration of the active sites with the strength sufficient to convert ethanol into ethylene. The higher the reciprocal of the slope $(1/S)$ the higher the activity towards ethylene formation. The following activity series can be obtained according to the previous criterion:

$$\text{SAPO-5}\ (1/S = 3.3) > \text{SAPO-11}\ (1/S = 0.5) > \text{AlPO}_4\text{-5}\ (1/S = 0.08) = \text{AlPO}_4\text{-11}\,.$$

This series is in close agreement with the acidity series derived from pyridine chemisorption and with the olefin selectivity series derived from Y_o-values.

It is evident that SAPO-5 contains a higher population of sites with the strength sufficient to catalyse the production of ethylene than SAPO-11. The question now arising is to know about the average acid strength of these two solids. Sanderson's intermediate electronegativity (S_{int}) and the partial charge on the hydrogen atoms (Z_H) have been proved to be good theoretical indexes for evaluating the integrated acid strength of zeolites and related materials [22]. On the other hand, a turnover-like number for the transformation of ethanol into olefin can also be calculated by combining the acidity and the catalytic experimental data. The latter parameter can, then, be taken as an experimental index of the average acid strength. Results of such calculations are given in table 5. As observed, SAPO-11 shows slightly higher average acid strength than SAPO-5, by applying both the theoretical and the experimental criterion. This result is in line with the higher SM2 + SM3 character of the mechanism of Si incorporation for the former structure, as deduced from the ^{29}Si MAS NMR experiments already discussed. Furthermore, the ratio hydrogen atomic fraction to silicon atomic fraction calculated from the empirical formula of table 5, yields 0.31 for SAPO-5 as compared to 0.17 for SAPO-11 in agreement, again, with the higher SM2 character of the Si substitution in SAPO-5.

It must be, however, emphasised that a general conclusion in relation to the relative acid strength of these structures cannot be drawn since, as has already been shown in the literature [10,13], both the silicon content and the atomic distribution within the framework are major influencing factors. Thus, Yang et al. [23], based on the position of the high-temperature peak-maximum during a NH_3-TPD experiment also observed a higher acid strength for SAPO-11 as compared to SAPO-5. Borade and Clearfield [18] found, with the aid of pyri-

Table 5
Theoretical and experimental parameters for evaluating the average acid strength

Catalyst	Py/UC [a]	B/(B + L)	B/UC [b]	Empirical formula	S_{int} [c]	Z_H [d]	TN [e] (s^{-1})
SAPO-5	0.84	0.73	0.610	$H_{0.050}Si_{0.16}AlP_{0.89}O_{4.10}$	4.20	0.166	0.040
SAPO-11	0.78	0.54	0.420	$H_{0.020}Si_{0.12}AlP_{0.99}O_{4.23}$	4.22	0.170	0.055
$AlPO_4$-5	0.39	0.44	0.014	$H_{0.014}AlP_{0.96}O_{3.92}$	4.21	0.168	0.022
$AlPO_4$-11	0.46	0.50	0.011	$H_{0.011}AlPO_4$	4.21	0.168	0.023

[a] Py/UC = molecules of pyridine per unit cell.
[b] B/UC = Brønsted sites per unit cell.
[c] S_{int} = Sanderson's intermediate electronegativity.
[d] Z_H = partial charge on the hydrogen atoms.
[e] TN = molecules of ethylene formed per Brønsted site per second.

dine-TPD technique, that samples of SAPO-11 and SAPO-5 had a similar acid strength. Campelo and coworkers [24], by contrast, using pyridine and aniline as probe molecules in both liquid and gas phase, observed that several samples of SAPO-5 contained acid sites of higher acid strength than SAPO-11. The latter authors, however, did not report the composition of their samples.

In order to explain the activity for the ethanol transformation into ether surprisingly observed for AlPO's, the total Brønsted fraction observed for these structures was incorporated in their corresponding empirical formula, used to calculate S_{int} and Z_H, as presented in table 5. As can be observed, the few Brønsted sites existing in these solids, probably as a result of structural defects, possess a theoretical average acid strength (Z_H values) comparable to that of SAPO's. The calculated turn-over numbers, very similar for AlPO's, were roughly half of those for SAPO's. Interestingly enough the sample of $AlPO_4$-5, having values of SSA and pore volume typical of highly pure and crystalline AFI materials, showed an acidity and catalytic behaviour almost identical to $AlPO_4$-11. This result seems to support the idea that the acidity and catalytic activity of $AlPO_4$-sieves are associated to structural OH groups instead to the presence of amorphous extra-framework materials. Choudhary and Akolekar [19] also observed a significant catalytic activity in cracking of hydrocarbons for a sample of $AlPO_4$-5 that they claimed to be highly crystalline. By comparison with an amorphous aluminophosphate, the previous authors showed that the crystalline $AlPO_4$-5 molecular sieve had much higher catalytic activity. The enhanced acidity of $AlPO_4$ molecular sieves relative to that of amorphous aluminophosphate materials has been explained in terms of concentration and confinement effects in the former [21].

4. Conclusions

The transformation of ethanol seems to follow closely a simple parallel kinetic scheme, for the formation of ether and ethylene over the catalysts and under the reaction conditions studied.

The ether formation can be thermodynamically limited for the ether formation at temperatures around 600 K. An absolute maximum ether yield of 0.39 was calculated at the limit when the formation of ethylene is completely inhibited. The formation of ethylene requires active sites of higher strength than those for the ether production. Consequently, the olefin-to-ether ratio measured, under kinetic regime, looks a good index for evaluating the relative fraction of such sites. The reciprocal of the slope of the experimental straight-lines derived from the parallel kinetic scheme, was shown to be an appropriate parameter for constructing an olefin selectivity series. This series was found to be in good agreement with the acidity series obtained from pyridine-TPD and pyridine-IR experiments.

Differences in the average active sites strength between SAPO-5 and SAPO-11, as experimentally determined from the turn-over numbers for the olefin formation (TN), were rationalised in terms of the hydrogen atoms average partial-charge (Z_H), taken as a theoretical index of average acid strength. Similarly, the same parameters, TN and Z_H, were also useful to explain the observed acidity and olefin production of AlPO's.

Evidence of structural influence over the product selectivity, as reported in the literature [1], was not found under the reaction conditions used in this work. In fact, the more open SAPO-5 structure showed lower selectivity towards the ether production, a bimolecular reaction requiring more spaciousness, than the medium-pore SAPO-11. Moreover, the selectivity pattern of $AlPO_4$-5 was almost identical to the one showed by $AlPO_4$-11

The degree of extension for the ethanol transformation into olefin, obtained from the equilibrium curve (Y_o-values), was found to be a good acidity indicator. The higher this value the higher the concentration of acid sites with the strength enough to promote the ethylene formation. The series observed using this criterion, was in excellent agreement with both the acidity one obtained from pyridine chemisorption and the olefin selectivity series derived from the reciprocal of the straight-lines slope resulting from the parallel kinetic scheme.

$AlPO_4$ structures, having mainly weak acid sites, were highly selective to ether showing an olefin restriction factor (ORF) of about 0.85.

Acknowledgement

This work was financially supported by CONICIT, project RPI-10001.

References

[1] C. de las Pozas, R. López-Cordero, J. Gonzalez-Morales, N. Travieso and R. Roque-Malherbe, J. Mol. Catal. 83 (1993) 145.
[2] M. Makarova, E. Paukshits, J.M. Thomas, C. Williams and K.I. Zamaraev, J. Catal. 149 (1994) 36.
[3] E. Derouane, J. Nagy, P. Dejaifve, J. van Hooff, B. Spekman, J. Védrine and C. Naccache, J. Catal. 53 (1978) 40.
[4] E. Costa, A. Uguina, J. Aguado and P. Hernández, Ind. Eng. Chem. Proc. Des. Dev. 24 (1985) 239.
[5] D. Marcano and L. Cortés, in: *Química Orgánica*, Vol. 1, ed. Reverté (1982) p. 494.
[6] D. Jingfa, Z. Guirong, D. Shuzhong, P. Haishui and W. Huaiming, Appl. Catal. 41 (1988) 13.
[7] A. Cobo and M. Mendes, Proc. X Iber. Simp. Catal., Vol II (1986) p. 627.
[8] S. Bun, S. Nishiyama, S. Tsuruya and M. Masai, Appl. Catal. 59 (1990) 13.
[9] H. Knözinger and R. Köhne, J. Catal. 5 (1966) 264.
[10] M. Alfonzo, J. Goldwasser, C.M. López, F.J. Machado, M. Matjushin, B. Méndez and M.M. Ramírez de Agudelo, J. Mol. Catal. 98 (1995) 35.
[11] C.A. Emeis, J. Catal. 141 (1993) 347.
[12] D. Stull, E. Westrun and G. Sinke: *The Chemical Thermodynamics of Organic Compounds* (Wiley, New York, 1969).
[13] J. Martens, P. Grobet and P. Jacobs, J. Catal. 126 (1990) 299.
[14] Chr. Minchev, Ya. Neinska, V. Valtchev, V. Minkov, T. Tsoncheva, V. Penchev, H. Lechert and M. Hess, Catal. Lett. 18 (1993) 125
[15] S. Elangovan, B. Arabindoo, V. Krishnasamy and V. Murugesan, J. Chem. Soc. Faraday Trans. 91 (1995) 4471.
[16] N. Tapp, N. Milestone, M. Bowden and R. Meinhold, Zeolites 10 (1990) 105.
[17] M.L. Cubeiro, C.M. López, A. Colmenares, L. Teixeira, M. Goldwasser, M.J. Perez-Zurita, F.J. Machado and F. González-Jiménez, Appl. Catal., submitted.
[18] R. Borade and A. Clearfield, J. Mol. Catal. 88 (1994) 249.
[19] V. Choudhary and D. Akolekar, J. Catal. 103 (1987) 115.
[20] M. Burgers and H. van Bekkum, Stud. Surf. Sci. Catal. 78 (1993) 567, and references 6, 8 and 9 therein.
[21] J. Horsley, E. Derouane, H. Foley, P. Jacobs and R. Szostak, in: *Nonaluminosilicate Molecular Sieves*, Study Number 4192 MS, Catalytica Studies Division (1992) p. 58.
[22] W.J. Mortier, J. Catal. 55 (1978) 138.
[23] L. Yang, Y. Aishen and X. Qinhua, Appl. Catal. 67 (1991) 169.
[24] J. Campelo, F. Lafoni and J. Marinas, in: *Proc. XIII Iber. Simp. Catal.*, Vol. II (1992) p. 1031.